SOILS AND FOUNDATIONS Vol. 39, No. 6, 103-116, Dec. 1999
Japanese Geotechnical Society

A MODEL FOR CLAY USING MODIFIED STRESS UNDER VARIOUS LOADING CONDITIONS WITH THE APPLICATION OF SUBLOADING CONCEPT

EHSANUL QUADER CHOWDHURY[i], TERUO NAKAI[ii], MASAYUKI TAWADA[iii] and SHOTARO YAMADA[iv]

ABSTRACT

In the conventional approach of elastoplastic modeling, using the invariants of ordinary stresses and strain increments can not properly consider the effect of intermediate principal stress on the strength and dilatancy of soils. A previously introduced modeling approach using modified stress (t_{ij}) can express the strength and dilatancy behavior of normally consolidated clay under generalized three-dimensional stress conditions. It has been verified that this modified stress approach closely simulates soil behavior under monotonic loading conditions. To express stress induced anisotropy, a kinematic hardening (in the stress ratio space) model for clay using modified stress has been proposed, which over predicts volumetric strain and does not show stabilization of strain during cyclic loading. To rectify those problems the evolution rule of the rotational variable has been modified and a subloading surface has been introduced in the model proposed in this paper. The applicability of the proposed model on normally or overconsolidated clay under monotonic or cyclic loading conditions is verified using triaxial, true triaxial and torsional shear tests.

Key words: clay, constitutive model, kinematic hardening, modified stress, stress history, subloading surface (**IGC**: D6)

INTRODUCTION

Conventional elastoplastic models use the invariants of ordinary stress tensor (σ_{ij}) as stress parameters, for example, p and q or σ_{oct} and τ_{oct} (Roscoe et al., 1963, 1968) where p is the mean and q is the deviator stress respectively, and σ_{oct} and τ_{oct} are the normal and shearing stresses on the octahedral plane. Use of these stress-parameters leads to the extended Mises strength criterion, which gives very high strength under triaxial extension and true triaxial stress conditions. Nakai and Mihara (1984) proposed a modified stress tensor (t_{ij}), which is a nonlinear function of ordinary stress tensor (σ_{ij}) and its invariants. Equations (1)–(4) show how the modified stress tensor (t_{ij}) can be obtained from an ordinary stress tensor. Here, it is noted that the principal directions of modified stresses are coaxial with the principal directions of ordinary stresses.

$$t_{ij}=a_{ik}\sigma_{kj} \tag{1}$$

In the above equation, a_{ij} is a dimensionless symmetric tensor obtained by reverse transformation from its principal values ($\hat{a}_{ij}$) as follows:

$$a_{ij}=Q_{im}Q_{jn}\hat{a}_{mn} \tag{2}$$

where, Q_{ij} is an orthogonal transformation that transforms ordinary stresses (σ_{ij}) to their principal values ($\hat{\sigma}_{ij}$).

$$\hat{\sigma}_{ij}=Q_{mi}Q_{nj}\sigma_{mn} \tag{3}$$

The principal values of a_{ij} are given by the following equation, which are also the direction cosines of the '*Spatial Mobilized Plane (SMP)*' (Matsuoka and Nakai, 1974; Nakai and Matsuoka 1983).

$$\left.\begin{array}{ll}\hat{a}_{ij}=\sqrt{I_3/(I_2\hat{\sigma}_{ij})} & \text{if, } i=j\\ \hat{a}_{ij}=0 & \text{else}\end{array}\right\} \tag{4}$$

After forming the modified stress tensor (t_{ij}), the scalars that represent the normal (t_N) and the parallel (t_S) components of stresses to the "*SMP*' are given by the Eqs. (5), (6). The stress ratio tensor x_{ij} and scalar stress ratio are given by Eqs. (7) and (8) respectively (Nakai et al., 1989(b), 1991, 1993).

$$t_N=t_{ij}a_{ij} \tag{5}$$

[i] Research Associate, Department of Civil Engineering, Nagoya Institute of Technology, Gokiso-cho, Showa-ku, Nagoya 466-8555.
[ii] Professor of Systems Management and Engineering, ditto.
[iii] Engineer, Nippon Telegraph and Telephone Corporation (Formerly graduate student of Nagoya Institute of Technology.).
[iv] Graduate student, Department of Civil Engineering, Nagoya Institute of Technology, Gokiso-cho, Showa-ku, Nagoya 466-8555, Japan.
Manuscript was received for review on July 21, 1998.
Written discussions on this paper should be submitted before July 1, 2000 to the Japanese Geotechnical Society, Sugayama Bldg. 4F, Kanda Awaji-cho 2-23, Chiyoda-ku, Tokyo 101-0063, Japan. Upon request the closing date may be extended one month.

$$t_S=\sqrt{(t_{ij}-t_N a_{ij})(t_{ij}-t_N a_{ij})} \quad (6)$$

$$x_{ij}=(t_{ij}-t_N a_{ij})/t_N \quad (7)$$

$$X=t_S/t_N=\sqrt{x_{ij}x_{ij}} \quad (8)$$

Use of the stress parameters t_N and t_S leads to Matsuoka-Nakai strength criterion (Matsuoka and Nakai, 1974, 1977) as in Eq. (9), which circumscribes the Mohr-Coulomb pyramid and gives strength close to the observed ones.

$$X=constant \quad \text{or} \quad I_1 I_2/I_3=constant \quad (9)$$

In the above equations I_1, I_2 and I_3 are the first, second and the third invariants of the ordinary stress tensor (σ_{ij}).

Since the principal directions of the modified stress t_{ij} and according to classical plasticity theory, principal directions of the plastic strain increments coincide with the principal directions of ordinary stresses, strain increment components conjugate to the stresses t_N and t_S are given by the following two equations respectively.

$$d\varepsilon^*_{SMP}=d\varepsilon_{ij}a_{ij} \quad (10)$$

$$d\gamma^*_{SMP}=\sqrt{(d\varepsilon_{ij}-d\varepsilon^*_{SMP}a_{ij})(d\varepsilon_{ij}-d\varepsilon^*_{SMP}a_{ij})} \quad (11)$$

Using the above mentioned stress and strain increment parameters, isotropic hardening clay and sand models have been proposed and verified by many triaxial and true triaxial tests (Nakai et al., 1984, 1986(a), 1986(b); Nakai, 1989(a)). These models were too simple and were not intended to express inherent or stress induced anisotropy of soils during cyclic loading.

Kinematic hardening models are usually used to simulate the behavior of stress induced anisotropy during cyclic loading. Generally, in the kinematic hardening models, it is assumed that the yield surface translates in the stress-space. The amount of translation of the origin of the yield surface relative to the origin of the stress-space is expressed by a tensor that possesses the dimension of stress and is known as back-stress. On the other hand, a few kinematic models allow the yield surface only to rotate in the stress-space by fixing the origin of the yield surface at the origin of the stress-space. The rotation of the yield surface can be viewed as the translation of the center of the yield surface on a deviator plane and can be expressed by a dimensionless tensor as the stress ratio tensor. The dimensionless tensor that expresses the center of the yield surface relative to the center of isotropic yield surface is called *back-stress-ratio* (Nakai et al. 1989(b), 1991, 1993).

Sekiguchi and Otha (1977) introduced anisotropy due to anisotropic consolidation in their model by allowing the yield surface to rotate a certain amount in the stress space. But they did not allow the yield surface to rotate further during shear. On the other hand Nakai et al. (1989(b), 1991, 1993) and Chowdhury and Nakai (1997) proposed models by allowing the yield surface to rotate continuously during loading process around the origin of the modified stress space to express the stress induced anisotropy during shear. They also formulated evolution rules for the central axis of the yield surface. The model we will be presenting in the next section will also use a similar description of anisotropy only its evolution rule is slightly different. In Eq. (12), n_{ij} is the tensor that determines the position of the central axis of the yield surface in the stress ratio space (x_{ij}). Nakai called tensor n_{ij} the *back stress ratio tensor*. Hashiguchi and Chen (1998) on the other hand linked n_{ij} with hardening and called it the *rotational hardening variable*.

$$x^*_{ij}=x_{ij}-n_{ij} \quad (12)$$

$$X^*=\sqrt{x^*_{ij}x^*_{ij}} \quad (13)$$

$$n=\sqrt{n_{ij}n_{ij}} \quad (14)$$

The original kinematic t_{ij}-clay (Nakai and Hoshikawa, 1991), more strictly a rotational model, did not link n_{ij} with hardening. Thus, the predicted volumetric strains were too high under cyclic loading. Also, it has been assumed that the interior of the yield surface is completely elastic as the conventional model. Thus, a smooth transition from elastic to elastic-fully-plastic state could not be obtained. In this paper n_{ij} is linked with hardening and a subloading surface is assumed for the smooth transition from elastic to elastic-fully-plastic state as the *subloading surface* model (Hashiguchi and Chen, 1998; Hashiguchi, 1980). In the next section we will formulate a model using the modified stress and strain increment parameters described in this section.

SUBLOADING AND ROTATIONAL HARDENING MODEL BASED ON THE t_{ij}

First of all we will define two yield surfaces named *normal yield surface* and *subloading surface* (Hashiguchi and Chen, 1998; Hashiguchi, 1980). In the conventional models the *yield surface* defines the region in which stress changes cause a completely elastic response and it remains stationary during elastic stress changes. But the interior of the *normal yield surface* is not completely elastic; elastoplastic response can be obtained due to loading within the *normal yield surface* but plastic strains are smaller in magnitude than the elastic-fully-plastic state. When the stress condition lies on the *normal yield surface*, an elastic-fully-plastic response is mobilized during loading. On the other hand the *subloading surface* always expands or contracts such that the current stress point lies on it but can never go beyond the *normal yield surface*. An elastic-fully-plastic response is obtained due to loading when the *subloading surface coincides* with the *normal yield surface*. Hashiguchi and Chen (1998) assumed that both the *normal yield surface* and the *subloading surface* translate and rotate in the stress space keeping similarity in their shapes. On the other hand, Asaoka et al. (1997) applied the subloading concept in the Cam clay model. But, they did not allow rotation or translation of the yield surfaces. We will assume that both the *normal yield surface* and the *subloading surface* pass through the origin and rotate, but do not translate in the modified stress space such that their central axes always coincide with each other. Both the yield surfaces al-

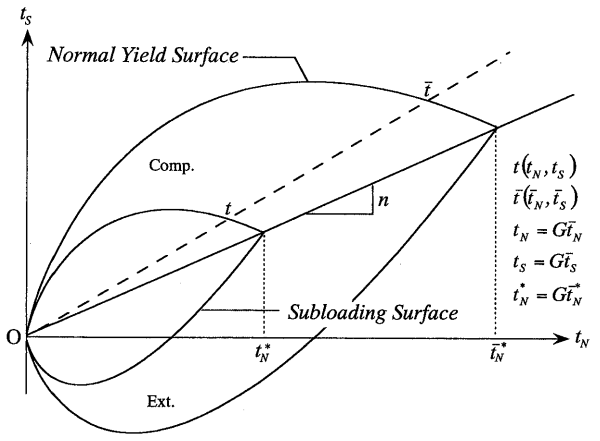

Fig. 1. Plane view of *normal yield surface* and *subloading surface*

ways keep similarity in their shapes.

Figure 1 is a simplified two-dimensional representation of a *normal yield surface* and a *subloading surface*. The similarity center of the yield surfaces always lie at the origin. Since, both of them pass through the origin, their central axes are coincident and are similar in shape. According to the definition of the similarity center, a straight line from the similarity center in any direction intersects both the surfaces at their conjugate points. In this figure current stress condition is at $t(t_N, t_S)$ and its conjugate stress condition on the *normal yield surface* is $\bar{t}(\bar{t}_N, \bar{t}_S)$. Actually, we would never calculate a point on the normal yield surface, which is conjugate to the current stress. This is because, we only need to know the size of the *normal yield surface*, which will be given in a few moments.

Let the following function give the general shape of the *normal yield surface*.

$$\bar{f}=\ln \bar{t}_N+\zeta(\bar{X}^*)-\ln \bar{t}_N^*=0 \tag{15}$$

In the above equation a superposed bar ('—') indicates stress conditions on the normal yield surface. On the other hand, stress conditions on the subloading surface (and the current stress condition) is given without a superposed bar. In Eq. (15), $\zeta(\bar{X}^*)$ is a monotonically increasing function of stress ratio, which will be defined explicitly in a later section. $\bar{t}_N^*$ is the size of the *normal yield surface* (Fig. 1) which is linked with the isotropic hardening variable ε_v^p (plastic volumetric strain) by assuming a linear relationship between ε_v^p vs. ln t_N as in the following equation.

$$\bar{t}_N^*=\bar{t}_{N0}^* \exp\left(\frac{\varepsilon_v^p}{C_t-C_e}\right) \tag{16}$$

where $\bar{t}_{N0}^*$ is the initial size of the *normal yield surface*, $C_t=\lambda/(1+e_0)$ and $C_e=\kappa/(1+e_0)$ are soil parameters. The compression and swelling indices on an e vs ln p plot are denoted as λ and κ respectively and e_0 is the reference void ratio.

The *subloading surface* is given by a similar function as the *normal yield surface* (Eq. (15)) as follows

$$f=\ln t_N+\zeta(X^*)-\ln t_N^*=0. \tag{17}$$

If the ratio of the sizes between the *subloading surface* and the *normal yield surface* is denoted by G $(0\leq G<1)$, then the following relations hold:

$$\left.\begin{aligned} t_N^*&=G\bar{t}_N^* \\ t_N&=G\bar{t}_N \\ t_S&=G\bar{t}_S \\ X^*&=\bar{X}^* \end{aligned}\right\}. \tag{18}$$

Equation (17) can be rewritten using Eqs. (16), (18) as follows:

$$f=\ln t_N+\zeta(X^*)-\ln G-\ln \bar{t}_{N0}^*-\frac{\varepsilon_v^p}{C_t-C_e}=0. \tag{19}$$

The differential form of the above equation is given by Eq. (20), which can be used as a consistency condition for the *subloading surface* by formulating proper evolution rules for n_{ij} and G.

$$df=\frac{\partial f}{\partial \sigma_{ij}}d\sigma_{ij}+\frac{\partial f}{\partial n_{ij}}dn_{ij}-\frac{dG}{G}-\frac{d\varepsilon_v^p}{C_t-C_e}=0 \tag{20}$$

It is assumed that the total strain increment is given by the following equation.

$$d\varepsilon_{ij}=d\varepsilon_{ij}^e+d\varepsilon_{ij}^p \tag{21}$$

The elastic constitutive equation follows the generalized Hooke's law for isotropic material.

$$d\varepsilon_{ij}^e=E^{-1}_{ijkl}d\sigma_{kl} \tag{22}$$

where,

$$E^{-1}_{ijkl}=\frac{1+\nu_e}{E_e}\delta_{ik}\delta_{jl}-\frac{\nu_e}{E_e}\delta_{ij}\delta_{kl} \tag{23}$$

or,

$$E_{ijkl}=\frac{E_e}{1+\nu_e}\delta_{ik}\delta_{jl}+\frac{\nu_e E_e}{(1+\nu_e)(1-2\nu_e)}\delta_{ij}\delta_{kl}. \tag{24}$$

In the above equations, Poisson's ratio ν_e is a soil parameter and E_e is the modulus of elasticity, which can be obtained from the slope (κ) of the unloading curve of isotropic consolidation test as:

$$E_e=\frac{3p(1-2\nu_e)(1+e_0)}{\kappa}=\frac{3p(1-2\nu_e)}{C_e}. \tag{25}$$

Though the original t_{ij}-clay model further decomposes the plastic strain increment to express the influence of loading direction. But for simplicity we assume here that the plastic strain is governed only by the flow rule in the t_{ij}-space:

$$d\varepsilon_{ij}^p=\Lambda\frac{\partial f}{\partial t_{ij}} \quad (\Lambda>0). \tag{26}$$

Scalar mtiltiplier Λ can be evaluated from the consistency condition of Eq. (20). But before that we need to define explicitly the evolution rules for the rotational hardening variable (n_{ij}) and the ratio between the *normal*

yield surface and the *subloading surface* (G).

Evolution Rule for 'n'

Simple evolution rules for the rotational variable using stress rates have been formulated previously (Nakai et al., 1989(b), 1991, 1993; Chowdhury and Nakai, 1997), but they can not express the change in anisotropy due to proportional loading. Inclusion of the deviator plastic strain increment in the evolution rule seems to obviate this defect. Also, paying attention to the evolution rule proposed by Hashiguchi and Chen (1998) following evolution rule for the rotational hardening variable is assumed:

$$dn_{ij}=k_r d\varepsilon_s^p \rho_{ij}. \tag{27}$$

The proportionality constant k_r is a soil parameter and the plastic deviator strain is given by

$$d\varepsilon_s^p=\sqrt{(d\varepsilon_{ij}^p-d\varepsilon_v^p\delta_{ij}/3)(d\varepsilon_{ij}^p-d\varepsilon_v^p\delta_{ij}/3)}. \tag{28}$$

The direction of movement of the yield surface in the stress ratio space is denoted by ρ_{ij} (Fig. 2), which is assumed as follows:

$$\rho_{ij}=X_r\frac{x_{ij}^*}{X^*}-n_{ij} \tag{29}$$

X_r is the size of the rotational limit surface and its geometric axis is coincident with the normal direction of the '*SMP*'. The central axis of the yield surface can not go beyond this surface. The central axis of the yield surface rotates in the modified stress space and approaches the conjugate line on the rotational limit surface as shear continues. For proportional loading with X=*const.* (anisotropic consolidation), the central axis of the yield surface approaches the loading path. Also, the above evolution rule can express diminishing of anisotropy of an anisotropically consolidated clay if consolidated isotropically to much higher confining pressure as observed in the triaxial tests. Substituting Eq. (29) in Eq. (27) we finally get the rotational evolution rule.

$$dn_{ij}=k_r d\varepsilon_s^p\left(X_r\frac{x_{ij}^*}{X^*}-n_{ij}\right) \tag{30}$$

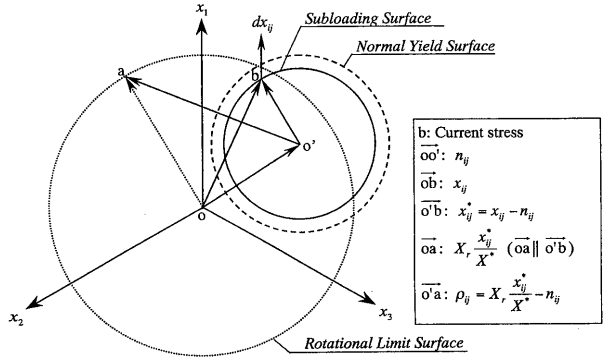

Fig. 2. ***Rotational Limit Surface*** **and direction of movement of central axis of** ***Subloading Surface*** **in stress ratio space**

Evolution Rule for 'G'

Hashiguchi and Chen (1998) and Hashiguchi (1980) proposed that the subloading surface approaches the normal yield surface monotonically during plastic loading process ($d\varepsilon_{ij}^p\neq 0$) as Eq. (31), which must satisfy the conditions of Eq. (33).

$$dG=Ud\varepsilon^p \tag{31}$$

$$d\varepsilon^p=\sqrt{d\varepsilon_{ij}^p d\varepsilon_{ij}^p} \tag{32}$$

$$\left.\begin{array}{lll} dG=+\infty & \text{if} & G=0 \\ dG>0 & \text{if} & 1>G>0 \\ dG=0 & \text{if} & G=1 \\ dG<0 & \text{if} & G>1 \end{array}\right\} \tag{33}$$

U in Eq. (31) should be such that it satisfy Eq. (33). Thus, U should have the following properties:

$$\left.\begin{array}{lll} U=+\infty & \text{if} & G=0 \\ U>0 & \text{if} & 1>G>0 \\ U=0 & \text{if} & G=1 \\ U<0 & \text{if} & G>1 \end{array}\right\}. \tag{34}$$

Though many functions could be assumed satisfying Eq. (34), we have adopted the following one, which is a continuous and monotonically decreasing function of G (Fig. 3).

$$U=-a\ln G \tag{35}$$

Substituting Eq. (35) in Eq. (31) we get the evolution rule for G.

$$dG=-ad\varepsilon^p \ln G \tag{36}$$

Substituting evolution rules (Eqs. (30) and (36)) and flow rule (Eq. (26)) in Eq. (20), and after simplification, one can get:

$$\Lambda=\frac{\dfrac{\partial f}{\partial\sigma_{ij}}E_{ijkl}d\varepsilon_{kl}}{h+\dfrac{\partial f}{\partial\sigma_{pq}}E_{pqrs}\dfrac{\partial f}{\partial t_{rs}}}. \tag{37}$$

Where

$$h=\frac{1}{C_t-C_e}\frac{\partial f}{\partial t_{kk}}-k_r\frac{\partial f}{\partial n_{ij}}\left(X_r\frac{x_{ij}^*}{X^*}-n_{ij}\right)\left\|\frac{\partial f^d}{\partial t}\right\| -\frac{a\ln G}{G}\left\|\frac{\partial f}{\partial t}\right\| \tag{38}$$

$$\left\|\frac{\partial f}{\partial t}\right\|=\sqrt{\frac{\partial f}{\partial t_{ij}}\frac{\partial f}{\partial t_{ij}}} \tag{39}$$

$$\left\|\frac{\partial f^d}{\partial t}\right\|=\sqrt{\left(\frac{\partial f}{\partial t_{ij}}-\frac{\partial f}{\partial t_{kk}}\frac{\delta_{ij}}{3}\right)\left(\frac{\partial f}{\partial t_{ij}}-\frac{\partial f}{\partial t_{kk}}\frac{\delta_{ij}}{3}\right)}. \tag{40}$$

The loading criterion can then be given by Eq. (41) or more simply by Eq. (42).

$$d\varepsilon_{ij}^p\neq 0 \quad \text{if} \quad \Lambda>0 \tag{41}$$

$$d\varepsilon_{ij}^p\neq 0 \quad \text{if} \quad \frac{\partial f}{\partial\sigma_{ij}}E_{ijkl}d\varepsilon_{kl}>0 \tag{42}$$

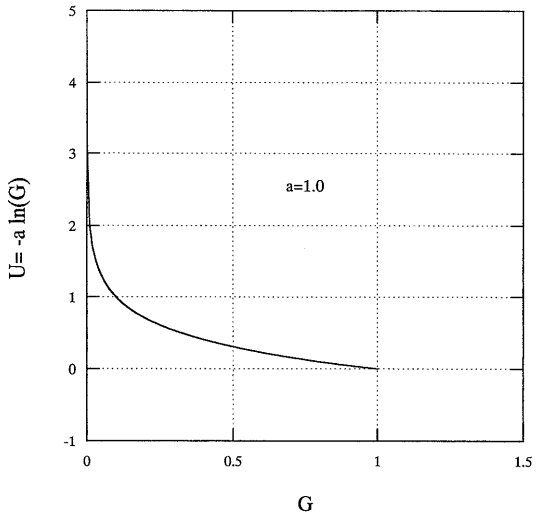

Fig. 3. Variation of U with G

The scalar Λ could have been evaluated using stress rate as Eq. (43). But it can not distinguish unloading from loading in the softening state. Thus, if Eq. (43) is used to evaluate Λ, then Eq. (41) can not be used as a generalized loading criterion but Eq. (42) still holds.

$$\frac{\dfrac{\partial f}{\partial \sigma_{ij}} d\sigma_{ij}}{h} \tag{43}$$

Finally stress increments can be related to strain increments as

$$d\sigma_{ij}=\left(E_{ijkl}-\frac{E_{ijrs}\dfrac{\partial f}{\partial t_{rs}}\dfrac{\partial f}{\partial \sigma_{pq}}E_{pqkl}}{h+\dfrac{\partial f}{\partial \sigma_{ab}}E_{abcd}\dfrac{\partial f}{\partial t_{cd}}}\right)d\varepsilon_{kl}. \tag{44}$$

Equations (33) and (34) look awkward, but they make sense if they are examined in conjunction with Eq. (37) or (43). If we unload to the similarity center (null stress for our model, $G=0$), the denominator of Λ is infinitely large. Thus, the magnitude of plastic strain is zero. That is, the response is elastic. If we continue shearing, magnitude of plastic strain increases monotonically until elastic-fully-plastic response is mobilized (*subloading surface* coincides with the *normal yield surface*, $G=1$). Hence, a smooth transition from elastic to elastic-fully-plastic state is possible.

Yield and Plastic Potential Functions

The yield and plastic potential functions of the conventional isotropic hardening t_{ij}-clay model (Nakai et al., 1986(a)) was given on the basis of a linear stress-dilatancy relation. The following equation is a further simplification by letting the slope of the stress-dilatancy curve to one as the original Cam-clay model.

$$g\equiv f=\ln t_N+\frac{X}{\mathrm{M}^*}-\ln t_{N1}=0 \tag{45}$$

To include the rotational hardening variable in the modeling, the above equation has been modified as Eqs. (46) and (47) to give the *normal yield surface* and *subloading surface* respectively. Here, we recall that $\bar{X}^*=X^*$ and $\bar{\mathrm{M}}_r^*=\mathrm{M}_r^*$.

$$\bar{g}\equiv\bar{f}=\ln \bar{t}_N+\frac{\bar{X}^*}{\bar{\mathrm{M}}_r^*}-\ln \bar{t}_N^*=0 \tag{46}$$

$$g\equiv f=\ln t_N+\frac{X^*}{\mathrm{M}_r^*}-\ln t_N^*=0 \tag{47}$$

Comparing Eqs. (46) and (47) with Eqs. (15) and (17) respectively, one gets $\zeta(\bar{X}^*)=(\bar{X}^*/\bar{\mathrm{M}}_r^*)$ and $\zeta(X^*)=(X^*/\mathrm{M}_r^*)$. In the above equations, M^* and M_r^* are the strength parameters corresponding to conventional isotropic and rotational hardening models respectively, which are functions of angle of internal friction (ϕ). In the next section we find a co-relation between M^* and M_r^*. The above functions are quite simple and one can avoid introducing new parameters. On the other hand, they have the demerit of having a singularity point at the tip.

EFFECT OF ROTATIONAL HARDENING VARIABLE ON THE STRENGTH

In the conventional isotropic hardening models, for example Cam-clay and t_{ij}-clay models, strength parameters M and M^* respectively are calculated using the angle of internal friction (ϕ) at critical state under triaxial compression condition.

$$\mathrm{M}=\frac{6\sin\phi}{3-\sin\phi} \tag{48}$$

$$\mathrm{M}^*=X_f+Y_f \tag{49}$$

Where, X_f and Y_f are the values of stress ratio (X) and dilatancy ($Y=d\varepsilon_{SMP}^{*p}/d\gamma_{SMP}^{*p}$) respectively at failure under triaxial compression condition, which can be obtained from the following equations:

$$X_f=\frac{\sqrt{2}}{3}\left(\sqrt{R}-\frac{1}{\sqrt{R}}\right) \tag{50}$$

$$Y_f=\frac{1}{\sqrt{2}}\frac{(1-\sqrt{R})}{(\sqrt{R}+0.5)} \tag{51}$$

$$R\equiv\frac{\sigma_1}{\sigma_3}=\frac{1+\sin\phi}{1-\sin\phi}. \tag{52}$$

For the t_{ij}-clay model, the explicit form of M^* depends on the shape of the plastic potential. In the above-mentioned models, shapes of the plastic potentials remain the same during shear. On the other hand, plastic potentials of the rotational hardening models, such as the one proposed in the last section change their shapes continuously as their central axes rotate. Thus, to fit the critical state predicted by the proposed model under monotonic loading (for example triaxial compression) to that of isotropic hardening conventional model, the strength parameter should be adjusted. This could also be achieved by adjusting the friction angle. But in that case

the friction angle loses its usual meaning. In this section we will find a co-relation between the strength parameters of ordinary and rotational hardening models.

For the conventional isotropic hardening t_{ij}-clay model, the direction of plastic flow can be obtained from Eq. (45) as follows:

$$\frac{\partial g}{\partial t_{ij}}=\frac{\partial g}{\partial t_N}\frac{\partial t_N}{\partial t_{ij}}+\frac{\partial g}{\partial X}\frac{\partial X}{\partial x_{kl}}\frac{\partial x_{kl}}{\partial t_{ij}} \tag{53}$$

$$\frac{\partial g}{\partial t_{ij}}=\frac{a_{ij}}{t_N}+\frac{\partial g}{\partial X}\frac{x_{kl}}{X}\frac{\partial x_{kl}}{\partial t_{ij}}. \tag{54}$$

For the proposed rotational hardening model, the normal to the plastic potential (Eq. (47)) is:

$$\frac{\partial g}{\partial t_{ij}}=\frac{\partial g}{\partial t_N}\frac{\partial t_N}{\partial t_{ij}}+\frac{\partial g}{\partial X^*}\frac{\partial X^*}{\partial x^*_{kl}}\frac{\partial x^*_{kl}}{\partial t_{ij}} \tag{55}$$

$$\frac{\partial g}{\partial t_{ij}}=\frac{a_{ij}}{t_N}+\frac{\partial g}{\partial X^*}\frac{x^*_{kl}}{X^*}\frac{\partial x_{kl}}{\partial t_{ij}}. \tag{56}$$

In deriving Eq. (56) we considered the fact that $(\partial n_{kl}/\partial t_{ij})=0$. Because n_{ij} is not a function of current stress,

$$\frac{\partial x^*_{kl}}{\partial t_{ij}}=\frac{\partial(x_{kl}-n_{kl})}{\partial t_{ij}}=\frac{\partial x_{kl}}{\partial t_{ij}}. \tag{57}$$

For the monotonic loading paths $(x_{kl}/X)=(x^*_{kl}/X^*)$ and hence Eq. (54) and Eq. (56) become equivalent if the following equation holds, which is the required condition to reach the critical state at the same stress condition as the isotropic hardening conventional models:

$$\frac{\partial g}{\partial X}=\frac{\partial g}{\partial X^*}. \tag{58}$$

Using the above relation from Eqs. (45) and (47) we can get

$$\mathrm{M}^*_r=\mathrm{M}^*. \tag{59}$$

Equation (59) implies that there is no effect of rotational hardening variable on the strength parameter for the plastic potential like Eq. (47). But, for other plastic potentials, the above relation may not be true. If the rotational hardening concept is introduced into the original and modified Cam-clay models, it can be shown that their strength parameters should be adjusted as Eq. (60) and Eq. (61) respectively:

$$\mathrm{M}_r=\mathrm{M} \tag{60}$$

$$\mathrm{M}_r=\sqrt{\mathrm{M}^2-\eta_r^2}. \tag{61}$$

In the above equations, M_r is the adjusted strength parameter and M is the usual strength parameter given by Eq. (48). For the plastic potential of the original Cam-clay there is no need to modify the strength parameter. On the other hand, strength parameter of the modified Cam-clay should be adjusted as Eq. (61). In this equation, η_r is the size of the rotational limit surface. In deriving the above co-relations between the strength parameters, we assume that the central axis of the plastic potential (yield surface) reaches its critical value (rotational limit surface) while stress condition reaches the critical state.

EXPERIMENTAL OBSERVATIONS AND NUMERICAL SIMULATIONS

To verify the proposed model triaxial, true triaxial and torsional shear tests on saturated and remolded Fujinomori clay are analyzed in this section. Analyses by the original kinematic t_{ij}-clay model (Nakai and Hoshikawa, 1991) are also presented where necessary for comparison. The following table shows the parameters of Fujinomori clay. The original kinematic t_{ij}-clay model has six parameters and the proposed model needs seven parameters, four of which are common to both models.

Parameter C_t for both the models is determined from the slope of the normal consolidation line on a semi logarithmic plot (ε_v vs. $\ln p$). Slope of the unloading curve C_e for the proposed model is also determined from the experimental observations. But, the original t_{ij}-clay and the kinematic t_{ij}-clay model use an empirical approach ($1-\kappa/\lambda=\mathrm{M}/1.75$, Karube, 1975) to determine C_e. Thus, the value of parameter C_e varies for the two models. Friction angle is calculated from triaxial compression tests. Poisson's ratio ν_e is assumed to be zero, though other reasonable values could be assumed for it because, in the case of soils, plastic strains are predominant and overall stress-strain response is not much affected by a slight variation in Poisson's ratio. A value for ν_e close to zero increases the value of coefficient of earth pressure at rest (K_0) under elastic unloading. In addition, it is usually believed that elastic shear strains are much lower than elastic volumetric strains and hence a higher value of shear modulus is desirable. The proposed model does not use parameters α and ξ. Methods for the determination of α and ξ have been described by Nakai and Matsuoka (1986a) and Nakai and Hoshikawa (1991) respectively. On the contrary, the proposed model uses new parameters a, k_r and X_r.

Parameter X_r ($<X_f$) determines the maximum rotation of the central axis of the yield surface. In addition, larger values of X_r will give lesser final plastic volumetric strain in monotonic tests (for example triaxial compression) on normally consolidated clay. Thus, it should be so chosen that the desired final plastic volumetric strain be obtained in the analysis of a triaxial compression test. This parameter is independent of parameters a and k_r. Thus

Table 1. Soil parameters of Fujinomori clay for various models

Parameter	Original model	Proposed model
$C_t=\lambda/(1+e_0)$	5.08×10^{-2}	5.08×10^{-2}
$C_e=\kappa/(1+e_0)$	1.12×10^{-2}	0.47×10^{-2}
φ'_{comp}	33.7°	33.7°
ν_e	0.0	0.0
α	0.7	x
ξ	0.2	x
a	x	0.20
k_r	x	0.30
X_r	x	0.30

X_r should be determined before a and k_r.

Parameter k_r controls the overall stress-strain response. Larger values of k_r cause the central axis to rotate at a faster rate towards its limiting value; thus the initial response is very sensitive to it. It should be adjusted by trial analyses of triaxial compression tests on normally consolidated clay until a good fit to the stress-strain curve is obtained.

Parameter a controls the peak stress ratio and stiffness of the stress-strain curve of overconsolidated clay. The larger the value of a, the higher will be the peak stress ratio and the stiffer will be the initial response of overconsolidated clay. But this parameter has no effect on the normally consolidated clay, so it should be determined after determining X_r and k_r by trial analyses of monotonic triaxial test on overconsolidated clay or from cyclic triaxial tests.

Stress paths followed in the monotonic triaxial and true thaxial tests (Nakai et al., 1986b) at constant mean stress are shown in Fig. 4. In this figure θ indicates the angle between the σ_a-axis and the corresponding radial stress path on the deviator plane. The angle $\theta=0°$ and $\theta=180°$ denote the stress paths of thaxial compression and extension respectively. Other stress paths ($\theta=15°$, $\theta=30°$ and $\theta=45°$) denote three different principal stresses.

Figures 5–9 show the observed and predicted responses in the triaxial and true triaxial tests. In these figures, principal strains are plotted against the stress ratio (q/p) and the volumetric strain (ε_v) is plotted against the major principal strain. Moreover, solid curves in these figures are the predicted responses by the proposed model, and broken curves are those by the original kinematic t_{ij}-clay model. Figures 5 and 6 correspond to the triaxial compression and extension tests respectively and Figs. 7–9 are those of the true triaxial tests. From these figures it can be seen that the original model overpredicts, but the proposed model closely predicts volumetric strains. This is achieved by linking rotational variable in the hardening process. Both the models predict strengths well but show relatively flexible stress-strain responses at low stress ratio because of the shape of the plastic potential, which is similar in shape to the original Cam-clay model.

Two simple cyclic triaxial tests at constant mean stress

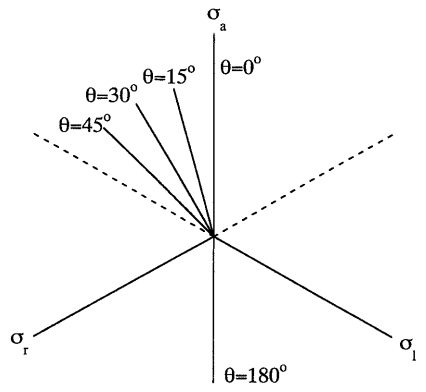

Fig. 4. Stress paths of triaxial and true triaxial tests on the octahedral plane

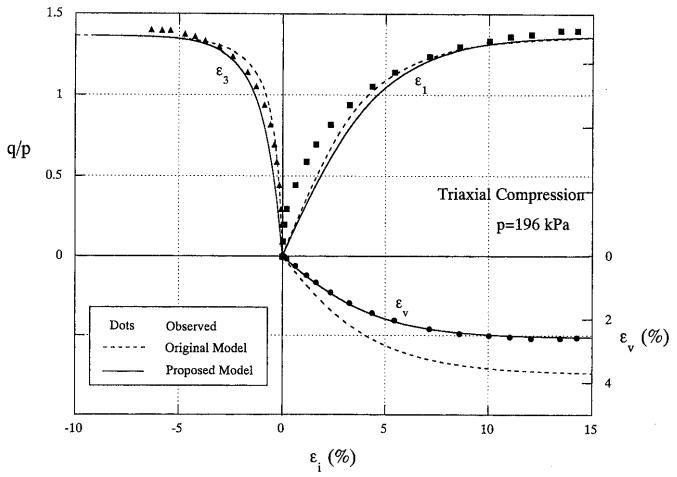

Fig. 5. Observed and predicted stress-strain relations for triaxial compression test

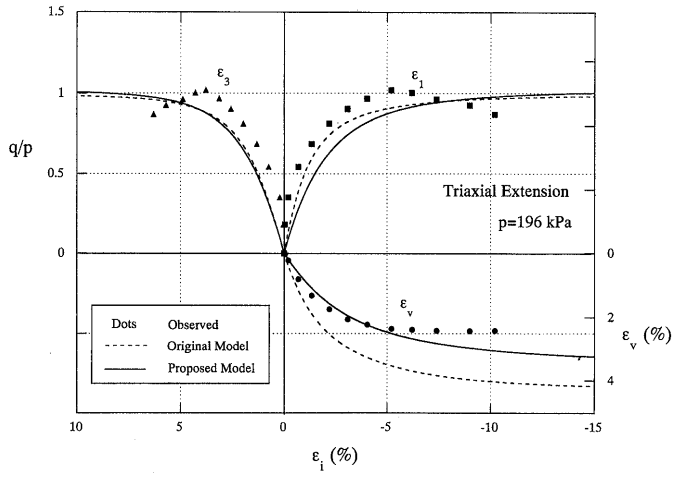

Fig. 6. Observed and predicted stress-strain relations for triaxial extension test

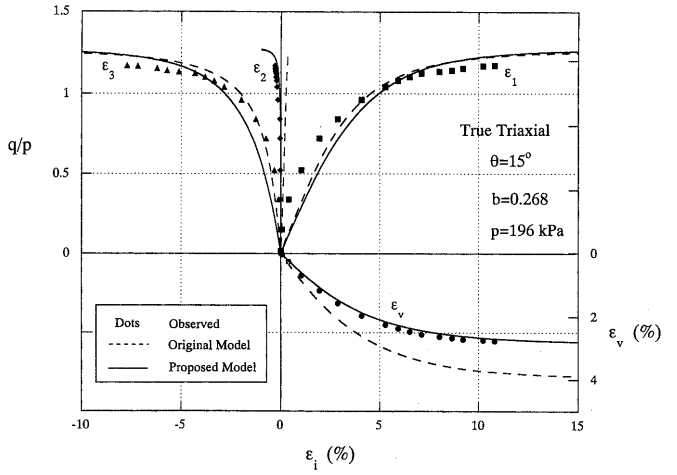

Fig. 7. Observed and predicted stress-strain relations for true triaxial test ($\theta=15°$)

(CY-1 and CY-2) are performed and corresponding analyses are shown in Figs. 10, 11. In these tests, soil samples are first sheared along compression and extension sides respectively to principal stress ratio of three ($\sigma_1/\sigma_3=3$), and then sheared in the reverse directions. Both the models show stress-induced anisotropy by predicting elastic responses at the initial part of reverse loading followed by elastoplastic responses. In case of the original model, stiffness falls drastically as soon as plastic loading occurs and hence gives very soft responses (Figs. 10(a), 11(a)). On the other hand, the proposed model shows a gradual drop in stiffness due to the consideration of a subloading surface. Also, it shows substantial reduction in volumetric strains (Figs. 10(b), 11(b)) during the reverse loading process but the original model shows excessive accumulation of volumetric strains. Two other features, softening and increase of strength due to cyclic loading, though not very prominent in these two tests, can be seen at the final stage of shearing. The proposed model shows a similar trend but the original model does not show such behavior.

Figure 12 shows the stress-strain diagrams of a constant amplitude ($\sigma_1/\sigma_3=3$, both in compression and extension) cyclic triaxial test at constant mean stress. As observed in the test, the proposed model shows stiffer responses in the successive loading loops. In other words, the magnitude of strains decreases and hence the area enclosed by each successive loop (Fig. 12(a)) decreases. Though the proposed model shows stabilization of volumetric strains (Fig. 12(b)), the rate is not as fast as it is ob-

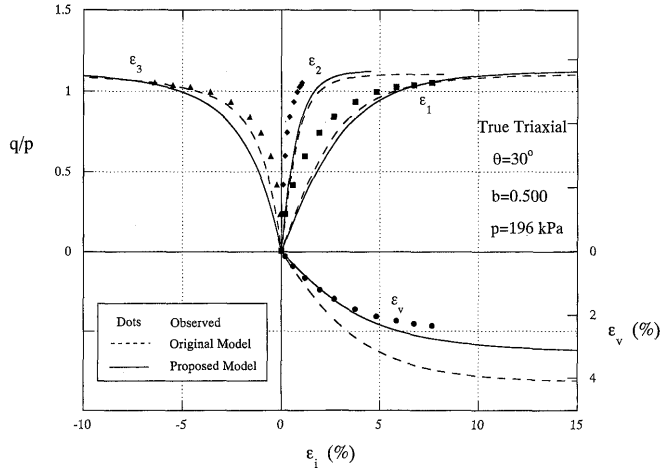

Fig. 8. Observed and predicted stress-strain relations for true triaxial test ($\theta=30°$)

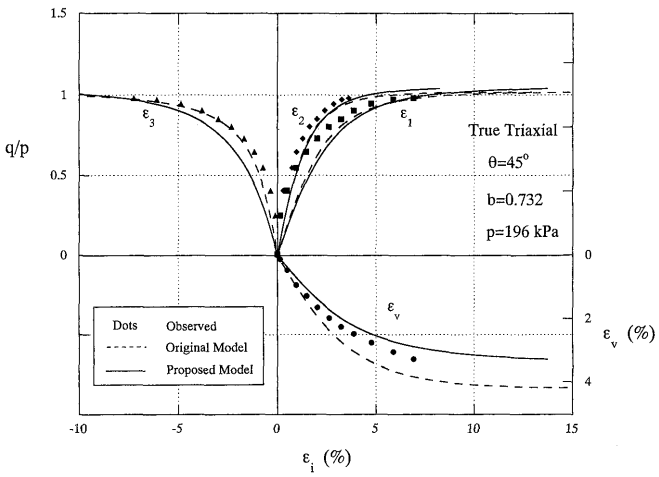

Fig. 9. Observed and predicted stress-strain relations for true triaxial test ($\theta=45°$)

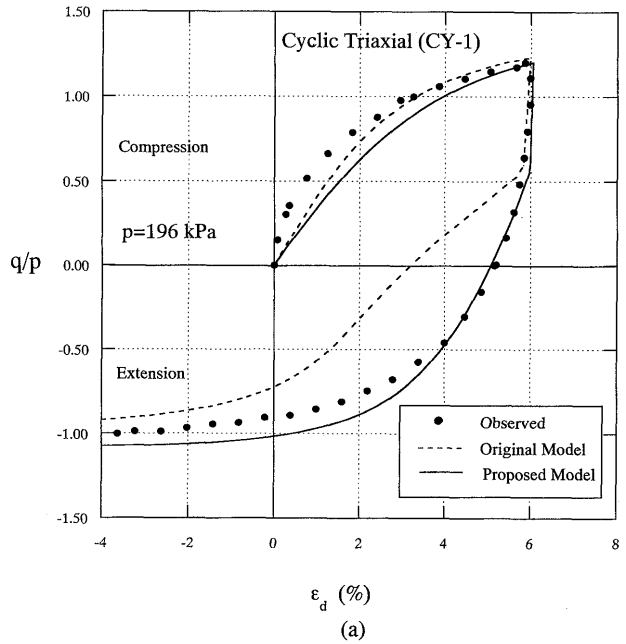

Fig. 10(a) Observed and predicted stress ratio vs. deviator strain relations of simple cyclic triaxial test (CY-1)

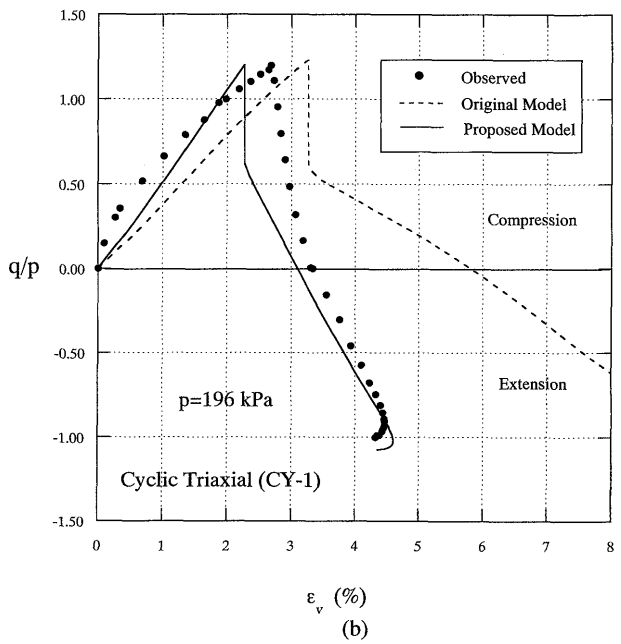

Fig. 10(b) Observed and predicted stress ratio vs. volumetric strain relations of simple cyclic triaxial test (CY-1)

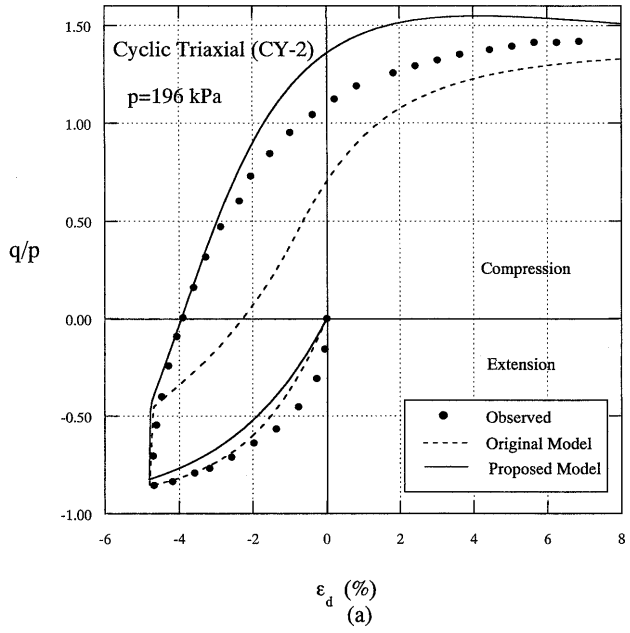

Fig. 11(a) Observed and predicted stress ratio vs. deviator strain relations of simple cyclic triaxial test (CY-2)

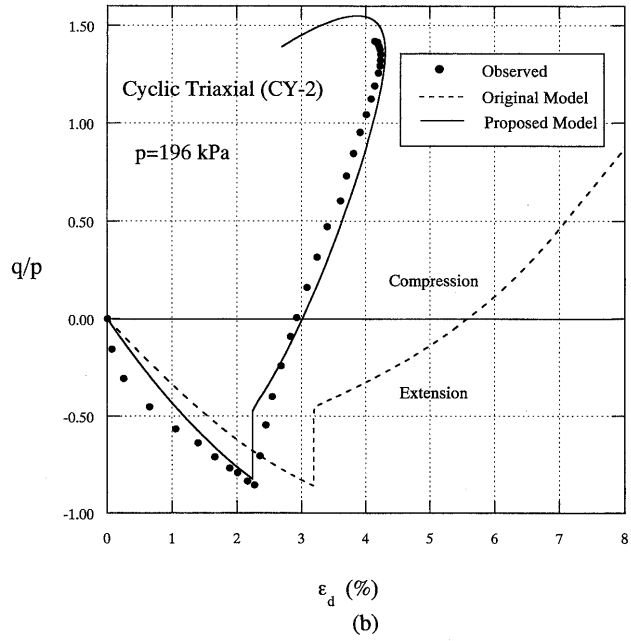

Fig. 11(b) Observed and predicted stress ratio vs. volumetric strain relations of simple cyclic triaxial test (CY-2)

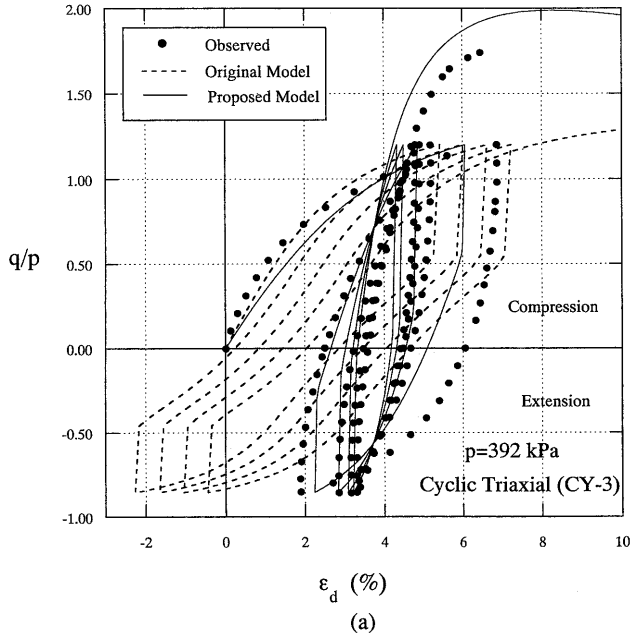

Fig. 12(a) Observed and predicted stress ratio vs. deviator strain relations of constant amplitude cyclic triaxial test (CY-3)

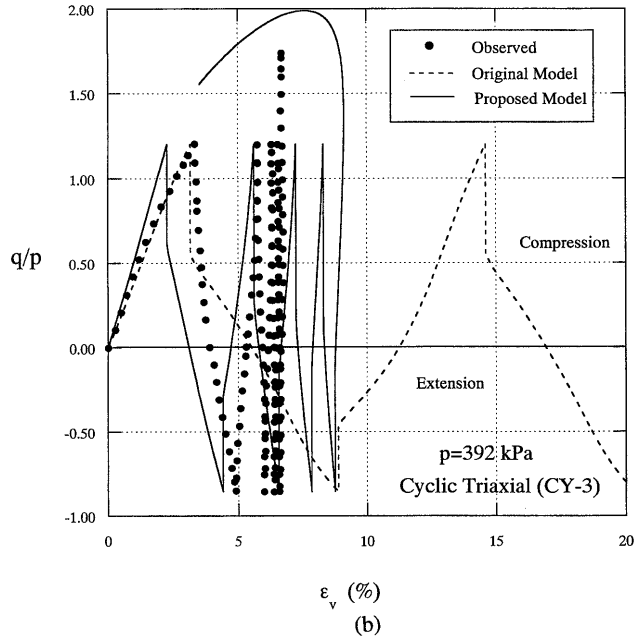

Fig. 12(b) Observed and predicted stress ratio vs. volumetric strain relations of constant amplitude cyclic triaxial test (CY-3)

served in the experiment. On the contrary, the original model repeats the same loop in both the figures. Also, the proposed model predicts substantial increase of strength at the final stage of shearing and shows softening. Experimental data also show increase in strength (compare to monotonic test) but softening could not be observed since it is a stress-controlled test. It is worth mentioning that performing strain controlled cyclic triaxial tests is very difficult especially under triaxial extension conditions. Thus the cyclic tests presented in these paper are carried out under stress controlled conditions.

Figure 13 shows the results of a variable amplitude cyclic triaxial test at constant mean stress. In these figures (Figs. 13(a), 13(b)) too, it can be seen that the proposed model predictions are quite representative of the experimental observations.

Figure 14 shows stress strain curves calculated by the proposed model for isotropically over consolidated clay under thaxial compression (Fig. 14(a)) and extension (Fig. 14(b)) with varying initial over consolidation ratio.

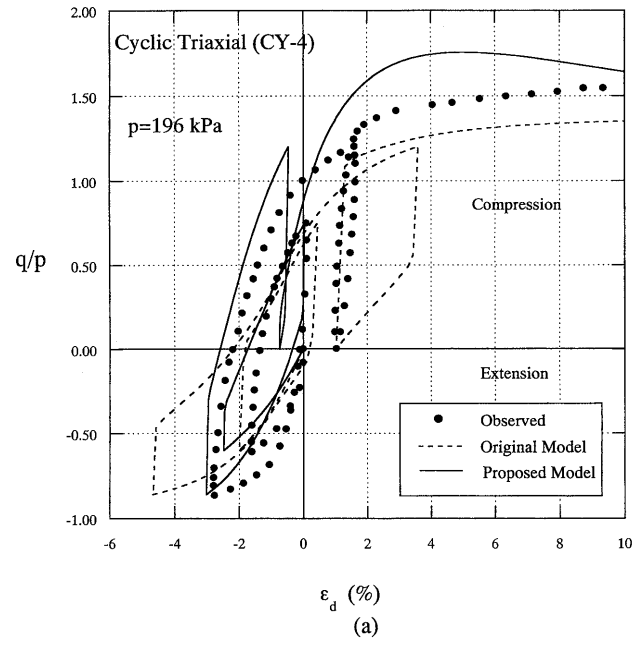

Fig. 13(a) Observed and predicted stress ratio vs. deviator strain relations of variable amplitude cyclic triaxial test (CY-4)

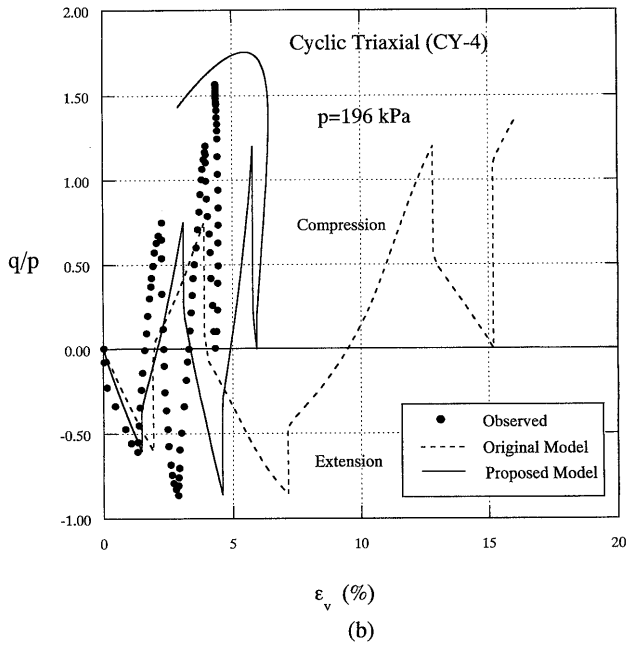

Fig. 13(b) Observed and predicted stress ratio vs. volumetric strain relations of variable amplitude cyclic triaxial test (CY-4)

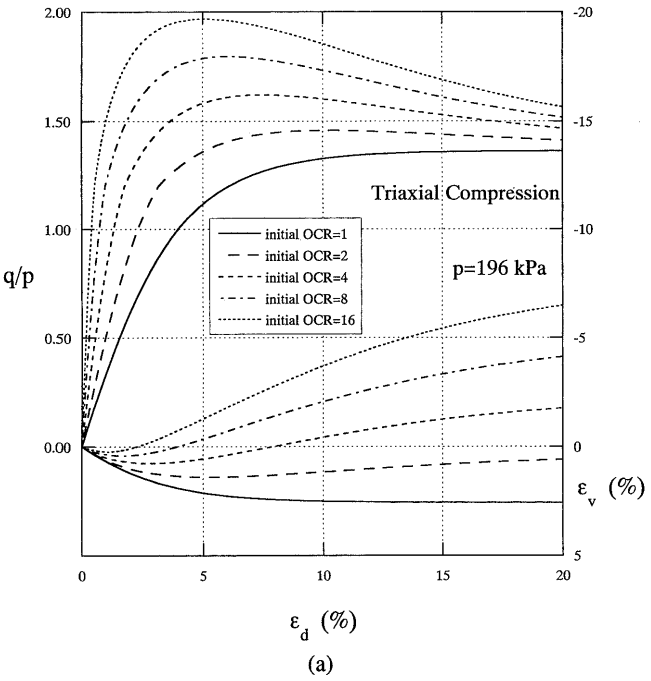

Fig. 14(a) Predicted stress-strain relations for overconsolidated clay with varying initial overconsolidation ratios under triaxial compression

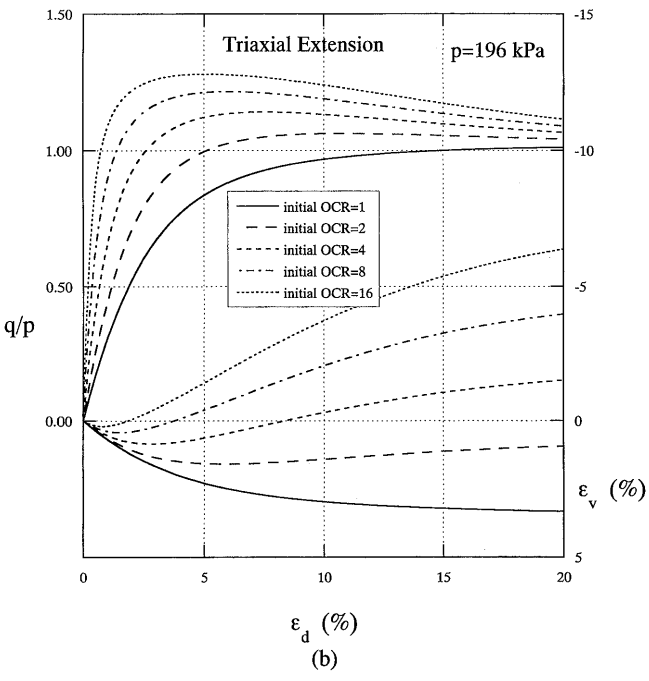

Fig. 14(b) Predicted stress-strain relations for overconsolidated clay with varying initial overconsolidation ratios under triaxial extension

These analyses are carried out using the same set of parameters as shown in Table 1. Since we have not sufficient data of triaxial tests at constant mean stress on overconsolidated Fujinomori clay samples, only analyses are shown in these figures. This has been done to emphasize the fact that the proposed model qualitatively simulates the characteristic features of overconsolidated clays. It can be observed from these figures that elastoplastic responses are obtained from the start of shearing but the conventional models give completely elastic response up to the peak. It is also observed that the strength increases with the increase of initial over consolidation ratio and stress-strain relations become stiffer. It is clear in these figures that the strength predicted under triaxial extension for a particular value of initial OCR is much less than the strength obtained in triaxial

compression for the same initial OCR, which is achieved through the use of modified stress t_{ij}. With the increase of initial OCR, clay samples become less contractive at the initial stage of shearing and more dilative as shear continues. After reaching the peaks, clay elements soften and eventually reach the critical state at large shear stains. The predicted trend qualitatively fits the observed trend reported before (Chowdhury and Nakai, 1997).

Conventional models (for example Cam clay and t_{ij}-clay model) are based on the assumption that there is no effect of stress path on the amount of hardening (plastic volumetric strain) if a certain state of stress is attained by elastoplastic loading. To be more specific, let us consider Fig. 15 in which isotropically consolidated clay samples (point A) are brought to the same stress condition (point F) through various stress paths. Then, all samples are sheared at constant mean stress. Conventional models give the same amount of volumetric strains at point F independent of the stress paths followed. But it is experimentally observed that the amount of volumetric strain varies depending on the stress paths followed with a definite trend. Figure 16(a) shows volumetric strains vary at point F in the range of three percent. It can be observed that the sample that experiences larger shearing strain shows lesser volumetric strains. In Fig. 16(a) path ABFG shows the least volumetric strain and shows the largest shearing strain (Fig. 16(b)). On the contrary, path AEFG shows maximum volumetric strain and minimum shearing strain at point F. The other two stress paths are also arranged in the same order. Analyses by the proposed model also show the same trend, although it shows a larger amount of shearing strain during anisotropic consolidation because of the shape of plastic potential. Analyses show that finally all samples reach the critical state and the volumetric strains are the same. Experimental observations also show a similar trend, except for path ABFG.

Now, we will show a few torsional shear test results on hollow cylindrical samples to simulate rotation of principal stress axes. Figures 17(a) and 17(b) show the stress paths followed in the tests on $(\sigma_a-\sigma_\theta)/2$ vs. $\tau_{a\theta}$ and on p vs. q planes respectively. In HC-1 and HC-2 samples are first sheared under triaxial compression ($\sigma_a>\sigma_\theta=\sigma_r$, $\tau_{a\theta}=0$) and extension ($\sigma_a<\sigma_\theta=\sigma_r$, $\tau_{a\theta}=0$) respectively, and then torque is applied to rotate the principal direc-

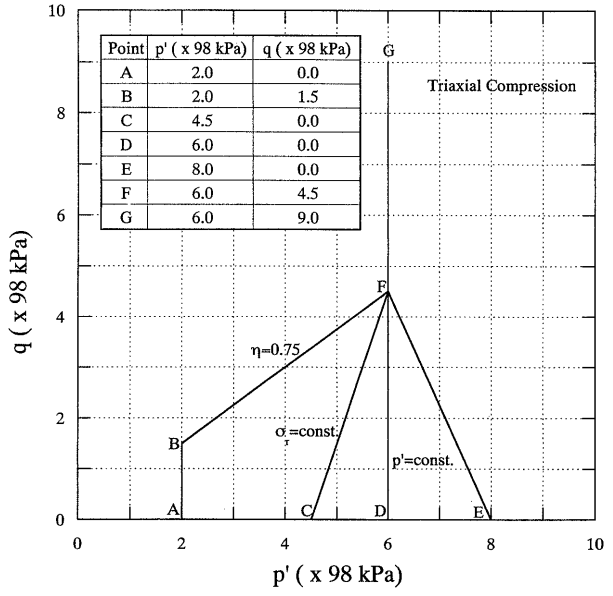

Fig. 15. Stress paths followed in triaxial compression tests to check the effect of stress paths on the stress-strain behavior

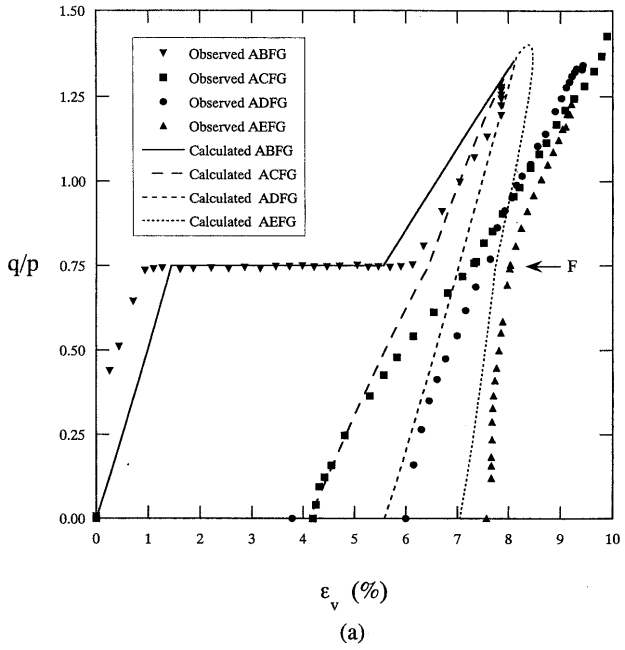

Fig. 16(a) Stress ratio vs. volumetric strain relations for four test paths and corresponding analyses by the proposed model

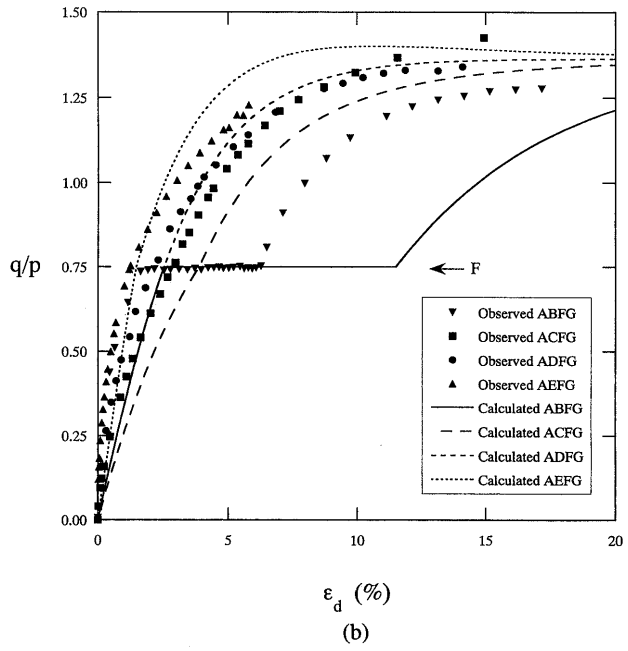

Fig. 16(b) Stress ratio vs. deviator strain relations for four test paths and corresponding analyses by the proposed model

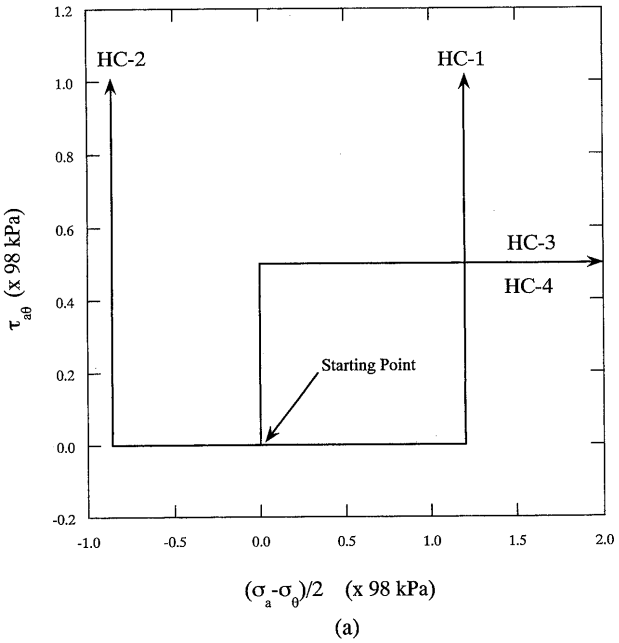

Fig. 17(a) Stress paths of the torsional shear tests on $(\sigma_a-\sigma_\theta)/2$ vs. $\tau_{a\theta}$ plane

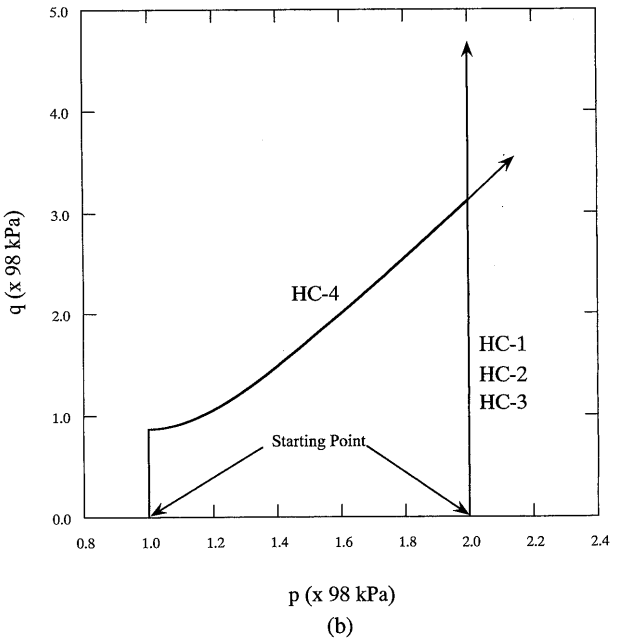

Fig. 17(b) Stress paths of the torsional shear tests on p vs. q plane

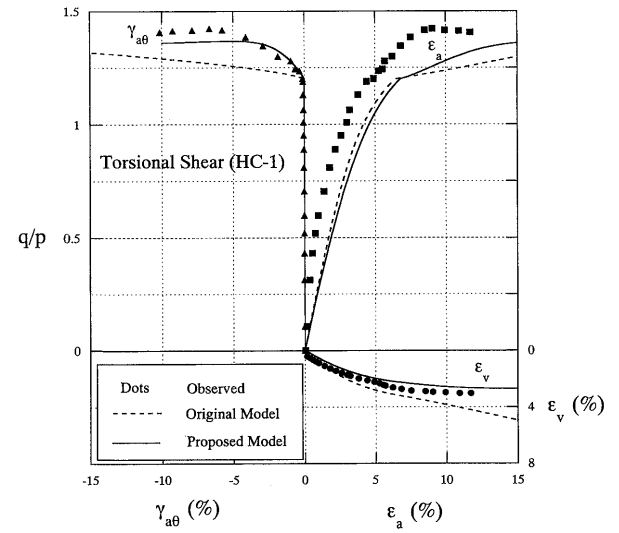

Fig. 18. Observed and predicted stress-strain responses of torsional shear test HC-1

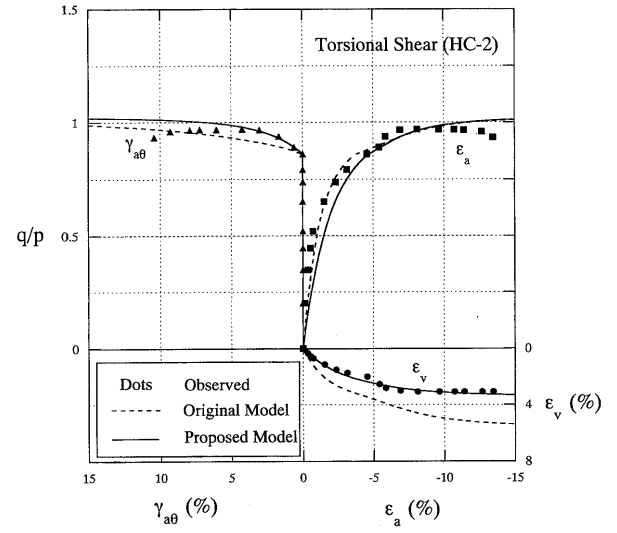

Fig. 19. Observed and predicted stress-strain responses of torsional shear test HC-2

tions. On the other hand, torque is applied first in HC-3 and HC-4, and then axial and radial stresses are varied to rotate the principal stress axes. The tests numbered HC-1, HC-2 and HC-3 are carried out at constant mean stress and in test HC-4, mean stress increases keeping constant torque. In these tests, shearing stress ($\tau_{a\theta}$) and average shearing strain ($\gamma_{a\theta}$) are calculated from the applied torque (T) and angular displacement ($\Delta\theta$ in degree) as follows:

$$\tau_{a\theta}=\frac{3T}{2\pi(r_o^3-r_i^3)} \tag{62}$$

$$\gamma_{a\theta}=\frac{\pi(r_o^3-r_i^3)}{270H(r_o^2-r_i^2)}\Delta\theta \tag{63}$$

where r_o and r_i are the outer and inner radius respectively and H is the height of the sample. Figures 18–21 show the stress-strain diagrams of these tests. Predictions by the original and the proposed models are also shown in these figures. It can be seen that at the start of rotation of principal directions, there is a little increase of stiffness in the stress-strain curve, which makes a kink in the observed stress-strain curves. Proposed model predictions match the observed stress strain behavior with a little soft response, which may be due to flat plastic potential used

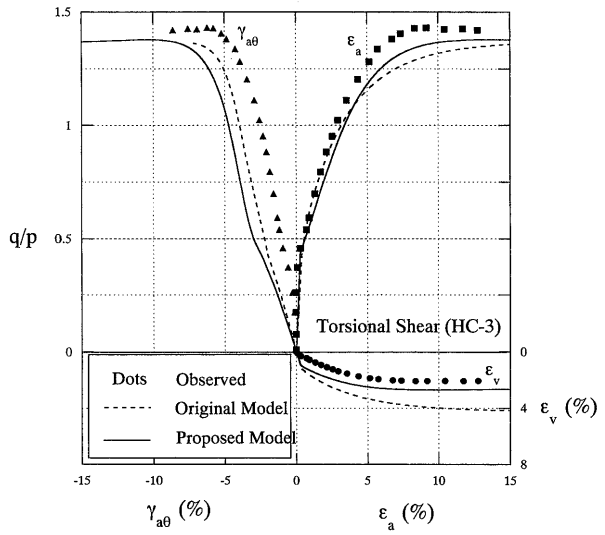

Fig. 20. Observed and predicted stress-strain responses of torsional shear test HC-3

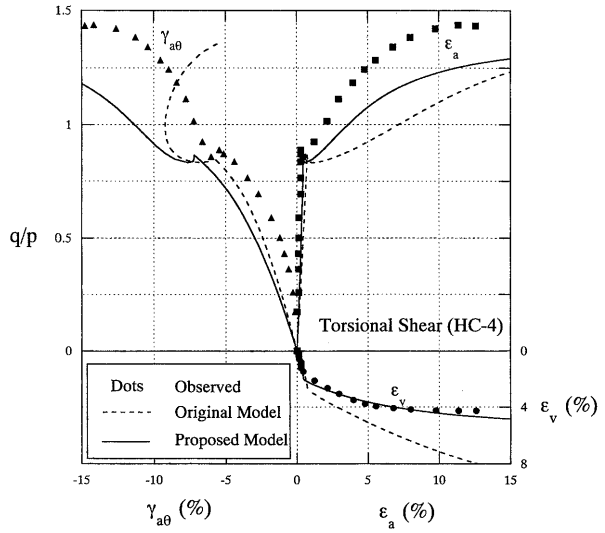

Fig. 21. Observed and predicted stress-strain responses of torsional shear test HC-4

in the model. In Fig. 21, predicted shearing strain ($\gamma_{a\theta}$) by the original model makes an about turn when axial stress increases while maintaining constant torque. However, the proposed model response is consistent with the observed behavior. This results from the difference of evolution rules of the central axes of the yield surfaces used in the models.

CONCLUSIONS

The model that is proposed in this paper differs from the original t_{ij}-clay or the kinematic t_{ij}-clay models in being able to predict cyclic or overconsolidated clay behavior properly by employing a subloading surface and modifying the hardening rule. In addition, the proposed model gives very consistent results under monotonic loading conditions. Thus, it can be considered as a model for generalized loading conditions in the analysis of boundary value problems.

Triaxial, true triaxial and torsional shear tests were performed to verify the proposed model. In modeling the behavior of geomaterials it is very common to use the non-associated flow rule. But, the proposed model shows very good agreement with the experimental results even using the associated flow rule in the t_{ij}-space. A very simple plastic potential (yield surface) with a sharp tip is considered in this paper. Consideration of a smooth plastic potential could increase the overall performance of the model, which is yet to be examined.

ACKNOWLEDEGEMENT

We would like to thank former graduate students of Nagoya Institute of Technology Mr. T. Masumoto and Mr. K. Iwahori for their support in carrying out experiments.

REFERENCES

1) Asaoka, A., Nakano, M. and Noda, T. (1997): "Soil-water coupled behavior of heavily overconsolidated clay near/at critical state," Soils and Foundations, Vol. 37, No. 1, pp. 13-28.
2) Chowdhury, E. Q. and Nakai, T. (1997): "A generalized model for clay under monotonic and cyclic loading conditions," Numerical Models in Geomechanics, NUMOG VI, Montreal, Canada, pp. 111-116.
3) Hashiguchi, K. and Chen, Z. P. (1998): "Elastoplastic constitutive equation of soils with the subloading surface and the rotational hardening," Int. J. Numerical and Analytical Methods in Geomechanics (in press).
4) Hashiguchi, K. (1980): "Constitutive equations of elastoplastic materials with elastic-plastic transition," J. Appl. Mech. ASME, Vol. 47, pp. 266-272.
5) Karube, D. (1975): "Nonstandard triaxial testing method and its problems," Proc. 20th Symp. on Soil Engrg., JSSMFE, pp. 45-60 (in Japanese).
6) Matsuoka, H. and Nakai, T. (1974): "Stress-deformation and strength characteristics of soil under three different principal stresses," Proc. JSCE, No. 232, pp. 59-70.
7) Matsuoka, H. and Nakai, T. (1977): "Stress-strain relationship of soil based on the SMP," Proc. Specialty Session 9, 9th Int. Conf. on SMFE, pp. 153-162.
8) Nakai, T. and Matsuoka, H. (1983): "Shear behaviors of sand and clay under three dimensional stress condition," Soils and Foundations, Vol. 23, No. 2, pp. 26-42.
9) Nakai, T. and Mihara, Y. (1984): "A new mechanical quantity for soils and its application to elastoplastic constitutive models," Soils and Foundations, Vol. 24, No. 2, pp. 82-94.
10) Nakai, T. and Matsuoka, H. (1986a): "A generalized elastoplastic constitutive model for clay in three-dimensional stresses," Soils and Foundations, Vol. 26, No. 3, pp. 81-98.
11) Nakai, T., Matsuoka, H., Okuno, N. and Tsuzuki, K. (1986b): "True triaxial tests on normally consolidated clay and analysis of the observed shear behavior using elastoplastic constitutive models," Soils and Foundations, Vol. 26, No. 4, pp. 67-78.
12) Nakai, T. (1989a): "An isotropic hardening elastoplastic model for sand considering the stress path dependency in three-dimensional stresses," Soils and Foundations, Vol. 29, No. 1, pp. 119-137.
13) Nakai, T., Fujii, J. and Taki, H. (1989b): "Kinematic extension of an isotropic hardening model for sand," Proc. NUMOG III, Niagara, pp. 36-45.

14) Nakai, T. and Hoshikawa, T. (1991): "Kinematic hardening model for clay in three dimensional stresses," Computer Methods and Advances in Geomechanics, Vol. 1, pp. 655–660.
15) Nakai, T., Taki, H. and Funada, T. (1993): "Simple and generalized modeling of various soil behavior in three-dimensional stresses," Modern Approaches to Plasticity, Elsevier Science Pub., pp. 561–584.
16) Roscoe, K. H., Schofield, A. N. and Thurairajah, A. (1963): "Yielding of clays in states wetter than critical," Géotechnique, Vol. 13, No. 3, pp. 211–240.
17) Roscoe, K. H. and Burland, J. B. (1968): "On the generalized stress-strain behavior of 'wet' clay," Engineering Plasticity, Cambridge University Press, U.K., pp. 535–609.
18) Sekiguchi, H. and Ohta, H. (1977): "Induced anisotropy and time dependency in clays," Proc. Specialty Session 9, 9th Int. Conf. on SMFE, Tokyo, pp. 229–238.